CHEMISTRY OF MATERIALS

ARTICLE

pubs.acs.org/cm

Shape-Controlled Growth and Shape-Dependent Cation Site Occupancy of Monodisperse Fe_3O_4 Nanoparticles

Chien-Hsin Ho,[†] Chih-Pin Tsai,[†] Chia-Chi Chung,[†] Chun-Ying Tsai,[‡] Fu-Rong Chen,[‡] Hong-Ji Lin,[§] and Chih-Huang Lai*,[†]

[†]Department of Materials Science and Engineering and [‡]Department of Engineering and System Science, National Tsing Hua University No. 101, Sec. 2, Kuang-Fu Road, Hsinchu, 30013 Taiwan

[§]National Synchrotron Radiation Research Center, Hsinchu, 300, Taiwan

Supporting Information

ABSTRACT: The shape control and formation mechanism of Fe_3O_4 nanoparticles (NPs) synthesized by a modified hot-injection method were investigated. Monodisperse Fe_3O_4 nanocubes terminated at {100} planes with the average size of 16.1 ± 0.9 nm were synthesized by injecting Fe precursor into reaction solution at 290 °C with a slow injection rate of 10 mL/h. When we increased the monomer concentration in solution by increasing the injection rate to 20 mL/h or doubling the precursor concentration with the same reaction time, the main terminated planes of Fe_3O_4 NPs became {100} and {110} planes leading to a rhombicuboctahedral shape. The shape of NPs was strongly affected by the monomer concentration and the intrinsic surface energy of Fe_3O_4. The shape-induced crystallographic orientation-ordered superlattices were obtained in both cubic and rhombicuboctahedral Fe_3O_4 NPs. On the other hand, the shape-dependent occupancy of the cation sites was clearly observed, measured by using X-ray magnetic circular dichroism (XMCD) spectra. The octahedral sites were occupied by more ferric ions, Fe^{3+}, when the shape of Fe_3O_4 NPs became cubic.

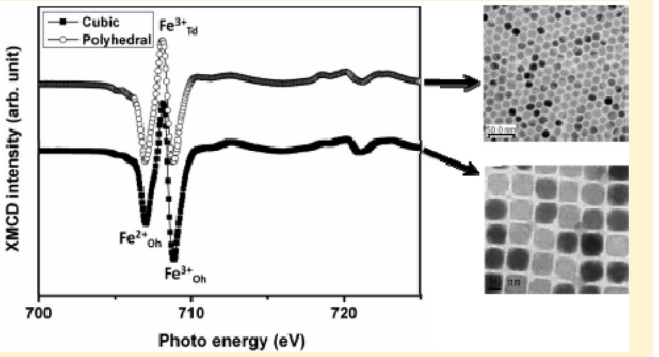

KEYWORDS: Fe_3O_4, nanocubes, shape control, hot injection, X-ray magnetic circular dichroism

INTRODUCTION

Tailoring the morphology of inorganic nanocrystal has long been an attractive field in nanoscience and technology.[1] In particular, magnetic nanoparticles (NPs) with unique size- and shape-dependent magnetic properties inspired an intensive exploration on their potential applications in the past decade.[2] Among those magnetic NPs, magnetite (Fe_3O_4) is one of the most well studied and widely used in biological applications such as magnetic resonance imaging (MRI), drug delivery, biosensor, magnetic separation, and medical diagnosis[3] because of its superparamagnetism under sub-20 nm and innate biological compatibility. Recently, some progress on synthesis of Fe_3O_4 NPs was focused on the shape control by solvothermal polyol process,[4] in which most of efforts were made on tuning the surfactants. For example, Kovalenko et al. synthesized the cubic Fe_3O_4 NPs by using oleate salts as surfactants to increase the concentration of "free" oleate ions which enhanced the surfactant effect.[4c] Yang and co-workers synthesized the Fe_3O_4 nanocubes by increasing the ratio of oleic acid (OA) to oleylamine and Fe precursors.[4d] Kim et al. presented Fe_3O_4 nanocubes with the size ranging from 20 to 160 nm by using OA only as a surfactant in reaction.[4f] Shaped Fe_3O_4 NPs such as nanocubes exhibit different terminated surface planes, on which the presence of ferrous (Fe^{2+}) and ferric (Fe^{3+}) ions may induce surface anisotropy and affect the fundamental magnetic properties such as blocking temperature and so forth.[5] In addition, the catalytic ability of Fe_3O_4 NPs was reported to be dominated by the type of the Fe cations on the exposed surface.[6] To explore the shape-dependent applications, the development of alternative methodologies for the facile and well-controlled synthesis of magnetic NPs as well as understanding of the shape formation remains an important challenge.

Herein, we demonstrate a modified hot-injection polyol process with a controlled injection rate to govern the shape of Fe_3O_4 NPs. The hot-injection method was first reported by Murray et al. for the synthesis of CdX (X = S, Se, Te) semiconductor NPs.[7] They instantly injected cold precursors into the hot reaction solution to generate the burst nucleation followed by nuclei-growth in the solution. Cozzoli and co-workers further modified the hot-injection method to synthesize the rod- and branch-like ZnSe nanocrystals by precisely controlling the precursor injection rate.[8] To our best knowledge, only few works have been reported on the synthesis of magnetic NPs with this modified hot-injection method.[9] In this study, we first

Received: September 25, 2010
Revised: January 7, 2011
Published: March 15, 2011

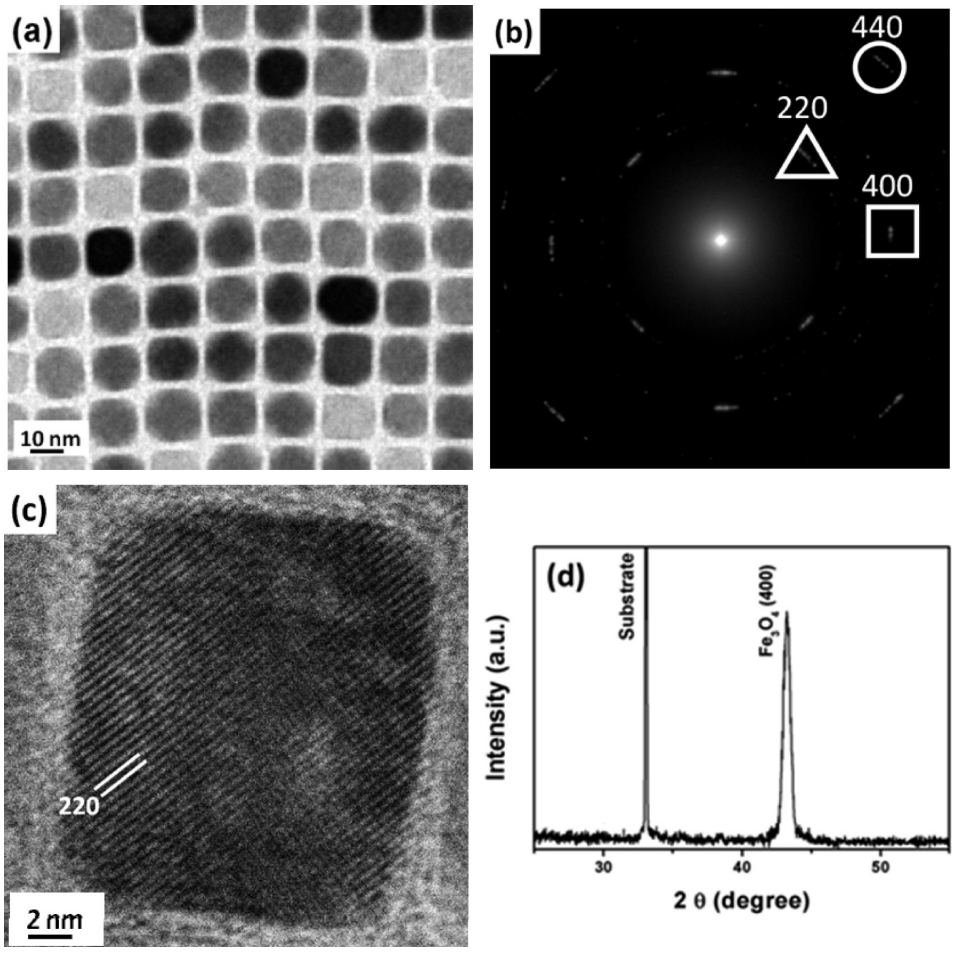

Figure 1. (a) TEM image of cubic Fe_3O_4 NPs, (b) corresponding SAED pattern of (a), (c) HRTEM image of a cubic Fe_3O_4 NP, and (d) XRD pattern of Fe_3O_4 nanocube array on a Si substrate.

successfully employed this method to fabricate shaped Fe_3O_4 NPs. By adjusting the monomer concentration, the uniform cubic and rhombicuboctahedral Fe_3O_4 nanocrystals with edge length of 16.1 ± 0.9 nm and 16.4 ± 1.1 nm, respectively, were synthesized in the benzyl ether solvent with the presence of oleylamine and oleic acid. The Fe_3O_4 nanocubes exhibited a terminated plane of {100} while the {100} and {110} terminated planes were observed in rhombicuboctahedral Fe_3O_4 NPs. We demonstrated that the shape evolution of Fe_3O_4 NPs was dominated by the Fe monomer concentration in the reaction solution and surface energy on various planes. We also showed that both cubic and rhombicuboctahedral NPs could be self-assembled into crystallographic orientation-ordered superlattices. Furthermore, shape-induced differential occupancy of the cation sites was revealed which might provide new avenues to applications, for example, catalyst,[6,10] by designing shaped Fe_3O_4 NPs.

EXPERIMENTAL SECTION

Materials. Iron(III) acetylacetonate ($Fe(acac)_3$, 99.9+%), 1,2-tetradecanediol (90%), oleic acid ($C_{17}H_{33}COOH$, 90%), oleylamine ($C_{18}H_{35}NH_2$, 99%), and benzyl ether ($C_{14}H_{12}O$, 99%) were purchased from Aldrich. All chemicals were used as received without further purification.

Synthesis of Cubic Fe_3O_4 NPs. All syntheses were performed using standard Schlenk line techniques. Typically, oleic acid (40 μL), oleylamine (40 μL), and 1,2-tetradecanediol (5 mmol) were dissolved in benzyl ether (15 mL) as the reaction solution, while $Fe(acac)_3$ (1 mmol) was dissolved in benzyl ether (5 mL) as the precursor solution with the concentration of 0.2 M. The reaction solution was dehydrated at 120 °C for 1 h, followed by being heated to the reflux temperature of 290 °C with a heating rate of 10 °C/min. Then the precursor solution was injected into the hot reaction solution at 290 °C with the injection rate of 10 mL/h. The fluctuation of reaction temperature was less than 5 °C during the injection process. After the injection was finished, the reaction solution was kept at 290 °C for 2 h and then naturally cooled to room temperature. Finally, the NPs were collected by centrifuge followed by being washed with ethanol and redispersed in hexane. This purified process was carried out for several cycles. The final product was stored in hexane. The experimental procedures are shown in Supporting Information Figure S1.

Formation Mechanism of Cubic Fe_3O_4 NPs. To understand how the cubic NPs were formed in this modified hot-injection method, we withdrew 0.1 mL of reaction solution for TEM analyses from the reaction bottle at 5 min, 10 min, 15 min, 20 min, 30 min, 1 h, 1.5 h, and 2 h after the precursor injection was triggered. Within the first 30 min, the precursor was still continuously injected into the reaction solution. The experimental procedures are also shown in Supporting Information Figure S1.

Surfactant Effect on Nanocube Synthesis. A total of 80, 160, and 400 μL of oleic acid and oleylamine each were dissolved in the

reaction solution containing benzyl ether (15 mL) and 1,2-tetradecanediol (5 mmol). The 0.2 M precursor solution including 1 mmol of $Fe(acac)_3$ was prepared in advance. Then the reaction solution was heated to 290 °C. The heating process and precursor solution injection rate (10 mL/h) were the same as those in the standard nanocube synthesis. The final products were collected by centrifuge followed by being washed with ethanol and redispersed in hexane.

Synthesis of Polyhedral Fe_3O_4 NPs by Adjusting the Monomer Concentration. Various precursor concentrations of 0.05 M, 0.1 M, and 0.3 M were prepared, while 0.2 M was used for the original condition of nanocube synthesis. The volume of precursor solution and the injection rate were kept at 5 and 10 mL/min respectively, and the reaction time was 2 h. For the precursor concentration of 0.3 M, the reaction time was further extended to 3 h to investigate how the shape was varied with precursor concentration in the solution. In addition, various injection rates of 2.5 mL/h and 20 mL/h were employed to compare with the original one of 10 mL/h. The rest of experimental parameters were the same.

Characterization of Materials. Transmission electron microscope (TEM) images were obtained by using JEOL JEM-1400 operated at 120 kV. The NPs were dispersed on amorphous carbon-coated copper grids for TEM studies. X-ray diffraction (XRD) patterns were detected by using Shimadzu XRD6000 with Cu Kα radiation. The XRD samples were prepared by dropping the NP dispersion on Si substrates. The substrates with NP assembly were moved into an airtight container in which solvent was slowly evaporated for 12 h. The Fe $L_{2,3}$-edge X-ray absorption spectroscopy (XAS) and X-ray magnetic circular dichroism (XMCD) measurements were performed at room temperature by using the total electron yield (TEY) mode at National Synchrotron Radiation Research Center (NSRRC) in Taiwan with an applied magnetic field of 1 T to fully saturate these NPs. The X-ray photoelectron spectroscopy (XPS) was also performed at room temperature at NSRRC.

RESULTS AND DISCUSSION

Modified Hot-Injection Polyol Processes for the Synthesis of Fe_3O_4 Nanocubes. The representative morphology of synthesized cubic Fe_3O_4 NPs characterized by TEM is shown in Figure 1a. The nanocubes with the average edge length of 16.1 ± 0.9 nm were self-assembled into a square packing array, and the size distribution shown in Supporting Information Figure S2 is only 5.6%. The corresponding selective area electron diffraction (SAED) pattern of the cubic NPs with square array shown in Figure 1b displays clear arced spots instead of rings, which are attributed to the formation of ordered crystallographic in-plane orientations.[11] The arced spots with fourfold symmetry are indexed as {220}, {400}, and {440} which indicate that the electron beam is along the [001] crystallographic orientation of Fe_3O_4. The crystalline structure and facets of Fe_3O_4 nanocubes were further verified by using a high-resolution TEM (HRTEM) image, shown in Figure 1c. It exhibits that the nanocubes are high-quality single-crystalline, and the distance of lattice fringes is 2.96 Å which corresponds to {220} lattice planes of Fe_3O_4 while the facet is {100}. The XRD pattern of the nanocube assembly displays only the (400) peak as shown in Figure 1d, which indicates that all the faceted planes of Fe_3O_4 {100} are preferentially parallel to the surface of the Si substrates. The (100) textured NP assembly was also found in the assembled $MnFe_2O_4$ nanocubes with the same cubic spinel structure and {100} faceted planes.[4a]

To investigate the formation mechanism of Fe_3O_4 nanocubes, an aliquot was withdrawn from the reaction solution at different durations of reaction for TEM analysis. Figure 2a−g shows TEM images of the intermediate NPs at the reaction times of 5 min, 10 min, 20 min, 30 min, 1 h, 1.5 h, and 2 h after starting the injection of precursor, respectively. The shape of Fe_3O_4 NPs was changed from a spheroidal to a polyhedral one before well-defined nanocubes were formed. The spheroidal Fe_3O_4 NPs were formed 5 min after the precursor injection (Figure 2a), and a quasi-isotropic growth was observed. In the subsequent 25 min injections (Figure 2b−d), the spheroidal shape changed to polyhedral or quasi-cubic. Finally, Fe_3O_4 NPs became well-defined nanocubes after the 30 min injection was finished. (Figure 2e−g). With the reaction time going on, the facet-selective

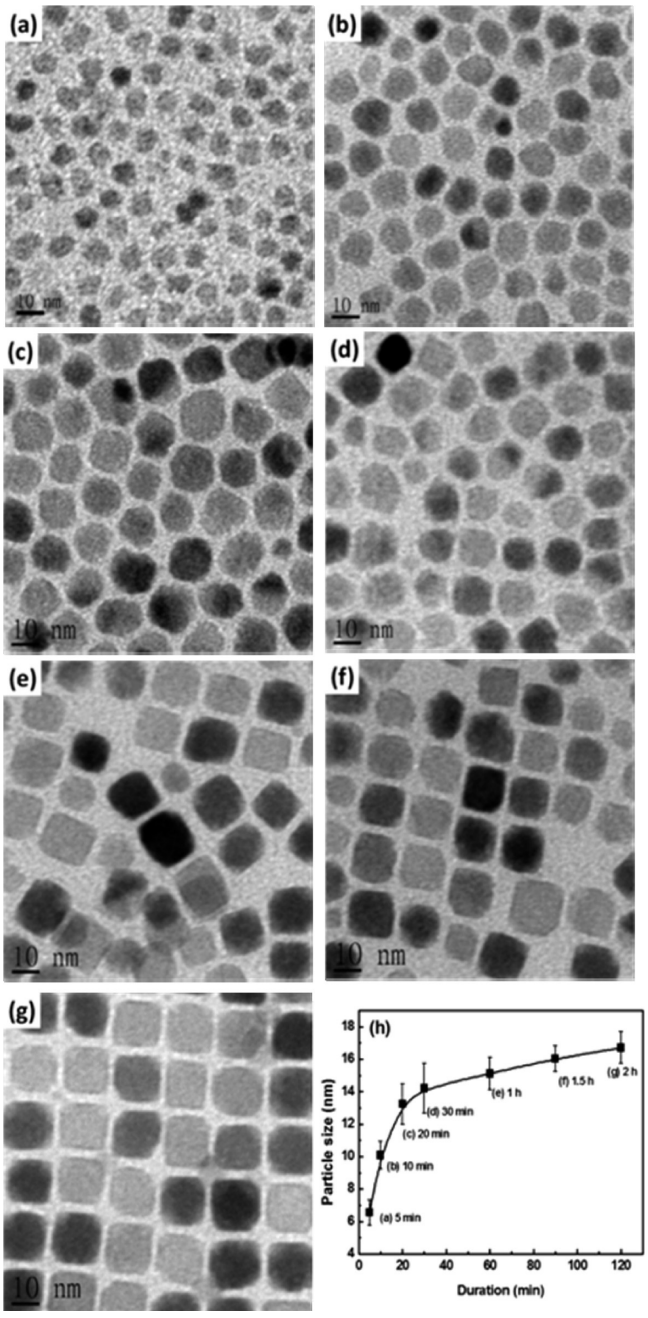

Figure 2. TEM images of Fe_3O_4 NPs withdrawn from the reaction solution at (a) 5 min, (b) 10 min, (c) 20 min, (d) 30 min, (e) 1 h, (f) 1.5 h, and (g) 2 h after the injection was triggered. (h) Dependence of the particle size on the duration time of reaction.

dx.doi.org/10.1021/cm102758u |*Chem. Mater.* 2011, 23, 1753–1760

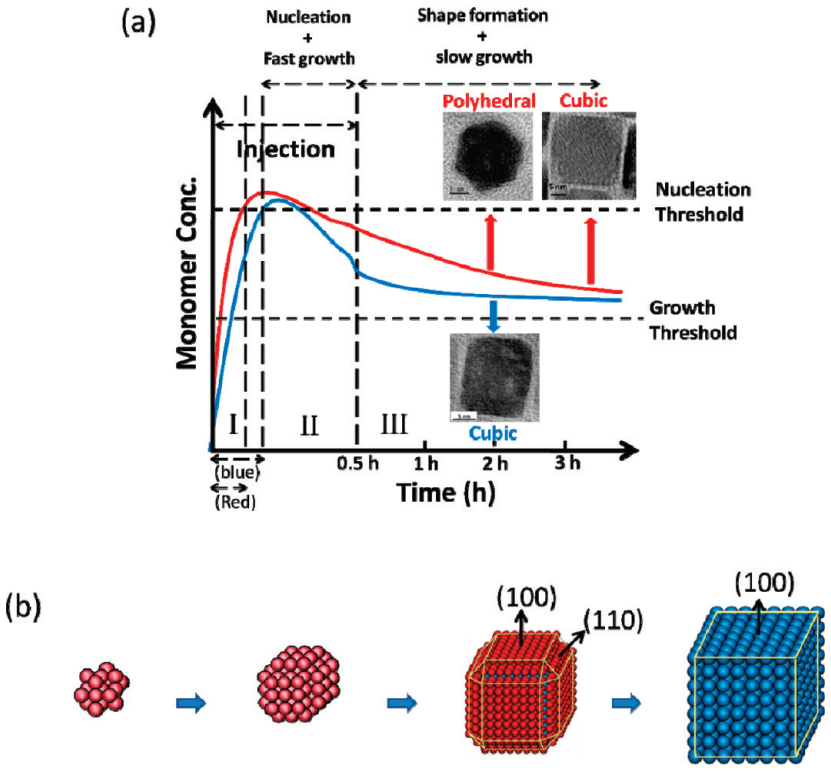

Figure 3. Schematic presentation of (a) concentration versus reaction time based on La Mer model for the modified hot-injection polyl processes (the blue and red lines represent the formation of nanocubes and nanopolyhedrons, respectively) and (b) the shape evolution for Fe_3O_4 NPs.

growth became more dominant at the latter stages of reaction. The progress of shape change usually accompanies the size variation. Figure 2h shows the size evolution versus the reaction time. It can be separated into two stages. In the first 30 min, the particle size steeply increases from 6.5 to 14.5 nm due to the continuous replenishment of monomers by the injection. After the 30 min injection, the particle size slightly increases to 16.1 nm which could be attributed to the monomer growth on the existing NPs and the Ostwald ripening.[12]

Many of the reported Fe_3O_4 nanocubes were synthesized at a high concentration of surfactants, which enhanced the surfactant effect.[4c−f] In our system, the surfactant concentrations were much lower than the reported ones.[4d,f] To investigate the surfactant effects in our modified hot-injection method, we increased the surfactant amount in the reaction solution. The changes of shape and size are shown in the TEM images of Supporting Information Figure S3. The size of the NPs decreased from ~16 nm (40 μL, oleic acid and oleylamine each, shown in Figure 1a) to ~10 nm (400 μL, shown in Supporting Information Figure S3c) with the increase of the surfactant concentration. The nanocubes can still be found in a surfactant concentration of 80 μL (Supporting Information Figure S3a) while relatively irregular shapes exist for NPs synthesized with higher concentration of surfactants (Supporting Information Figures S3b for 160 μL and S3c for 400 μL). In previous reports, the Fe_3O_4 nanocubes were synthesized by using a heating-up method;[4d,f] that is, the precursor was injected at room temperature and the whole solution was heated up to the reaction temperature. The heating-up synthesis typically uses either surfactant type or concentration to control the shape of the NPs. The high surfactant concentration of OA with the carboxylic group is selectively bonded onto the low energy facets, which shows the strong surfactant effect on particle shaping.[4d,f] However, we obtained irregular NPs by increasing the surfactant concentration, which suggested that the surfactant effect might not be a major factor in our modified hot-injection synthesis. In addition to using the surfactants for the shape control, several theoretical and experimental results of shaped semiconductor nanocrystals have been reported by tuning the monomer concentration.[13] In our slow-rate hot-injection synthesis, the monomer concentration in the solution can be properly controlled by injection rate or precursor concentration, so even with the low-concentration surfactants the shape can be tuned by adjusting the monomer concentration.

The shape formation process of the modified hot-injection method can be described by using the La Mer model[14] as shown in Figure 3a. The monomer concentration was gradually increased at the beginning of injection (period I, less than 5 min). During this period, the injected precursor was decomposed and started to accumulate. With the continuous supply of the precursor, the monomer concentration was increased and reached the minium nucleation concentration (a supersaturation level, start of period II). As long as the nucleation occurred, the monomer concentration was rapidly decreased to below the nucleation threshold, and the monomer was continuously consumed for subsequent particle growth. The slowly replenished monomers from the injected precursor with a low injection rate during the latter stage of period II provided adequate amounts of monomers, but not over the minimum nucleation concentration in the solution, which ensured the growth occurred on the existing nuclei without further nucleation. The process in this period included necleation and fast particle growth. The corresponding TEM images of NPs are shown in Figure 2a−d for the synthesis with the injection rate of 10 mL/h. After the injection

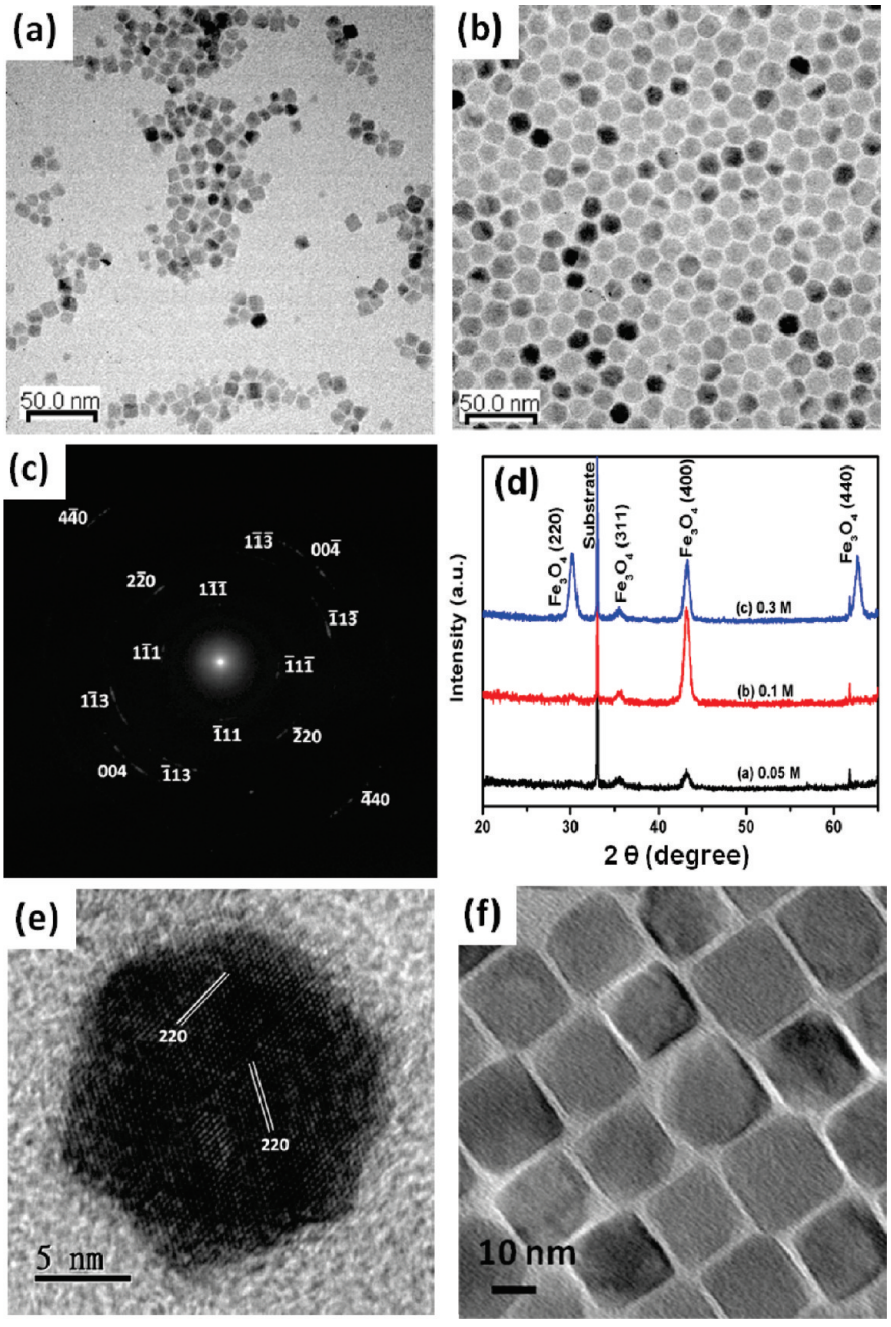

Figure 4. (a) and (b) are TEM images of Fe_3O_4 NPs synthesized with different precursor concentrations of 0.05 and 0.3 M, respectively. The reaction time is 2 h. (c) The corresponding SAED pattern of (b). (d) XRD patterns for corresponding samples. (e) HRTEM image of the polyhedral Fe_3O_4 NP on the zone axis of Fe_3O_4 [111] and (f) TEM image of Fe_3O_4 NPs synthesized with the reaction time of 3 h. Both (e) and (f) were synthesized with the precursor concentration of 0.3 M.

was finished (beginning of period III), no new monomers were supplied in the reaction solution. The monomer concentration was gradually decreased in the period III for further growth of NPs.

The shape evolution toward a stable cubic shape should be due to surface dissolution and reconstruction. The monomer concentration in reaction solution affects rates of both dissolution and reconstruction. Furthermore, the dissolution and reconstruction preferably occur at the facets with high surface energy. The facet growth rate was strongly associated with the intrinsic surface energy, surface ligands from surfactants, and monomer concentration in the reaction solution. As we discussed previously, the surfactant effect may not be a major effect in our synthetic system; therefore, the facet growth rate was governed by the intrinsic surface energy and the monomer concentration. For spinel oxides, the {100} planes showed the lowest surface energy while the {111} planes had the highest one among {100}, {110}, and {111} planes.[15] When the monomer concentration was high, the growth rates on various planes are fast that the differential growth is not significant, leading to a spheroidal shape (Figure 2a). The gradual decrease in monomer concentration triggered the difference in the growth rate of various planes,

dx.doi.org/10.1021/cm102758u |*Chem. Mater.* 2011, 23, 1753–1760

resulting in a polyhedral shape (Figure 2b−d). The TEM image shown in Figure 2d revealed that the shape was still not regular at the end of period II (at 30 min), which stongly suggested that the final shape was determined during period III. When the monomer concentration was low at the end of period II (for example, the blue curve in Figure 3a), the promoted facet-selective growth in period III, which depended on the differential intrinsic growth rate and dissolution/reconstruction on different planes, determined the final shape. The limited monomers preferentially grew on the planes with higher surface energy, such as {111} and {110} planes, to reduce the total energy. Consequently, the growth rate of the {100} planes became slowest due to their lowest surface energy in spinel oxides, leading to the formation of nanocubes with the terminated {100} planes (Figure 2e−g and Figure 1c). The possible mechanism of shape evolution for Fe_3O_4 NPs is schematically depicted in Figure 3b. Because controlling the monomer concentration is important in this method, the hot solution provides enough thermal energy for immediate decomposition of injected precursors and facet growth on the existing nuclei.

Synthesis of the Polyhedral Fe_3O_4 NPs. According to the previously proposed formation mechanism of nanocubes, the facet-selective growth became significant for the limited monomer concentrations. Therefore, it would be important to examine how the monomer concentration affected the shape of the NPs. We changed monomer concentrations by adjusting the precursor concentration or the injection rate of precursor. Figure 4a,b shows the TEM images of Fe_3O_4 NPs synthesized with the precursor concentration of 0.05 M and 0.3 M, respectively, while the concentration of 0.2 M was used in the original synthesis. Cubic NPs can be still observed at low precursor concentrations of 0.05 and 0.1 M (Supporting Information Figure S4), even though the particle size was decreased to 9 nm at the precursor concentration of 0.05 M. However, the shape of NPs prepared with high precursor concentration of 0.3 M after 2 h of reaction became polyhedral with a slightly enlarged size of 16.4 ± 1.1 nm, compared to those nanocubes synthesized with precursor concentration of 0.2 M. The polyhedral Fe_3O_4 NPs were self-assembled into a hexagonal packing array (Figure 4b), and their corresponding SAED pattern displays arced spots instead of rings, shown in Figure 4c. These arced spots with twofold symmetry are indexed as {111}, {220}, {311}, {400}, and {440} planes, indicating the polyhedral NP array also has ordered in-plane crystallographic orientations. This arced spot pattern is consistent with the simulated pattern with the zone axis of Fe_3O_4 [110]. In addition, both cubic and polyhedral NPs display the texture-like assemblies on Si substrates in XRD patterns, shown in Figure 4d. The assemblies of cubic Fe_3O_4 NPs, synthesized with the precursor concentration of 0.05 and 0.1 M, display the strongest Fe_3O_4 (400) peak. However, the XRD pattern of polyhedral NPs, synthesized with the precursor concentration of 0.3 M, reveals that intensities of both the (220) and the (440) peaks become comparable to that of the (400) peak. This result indicated that both {110} and {100} planes of polyhedral Fe_3O_4 NPs were preferentially parallel to Si substrates, which implied {110} and {100} planes were the major faceted planes of the polyhedral NPs. The HRTEM image (Figure 4e) reveals that the 2D projection of the polyhedral Fe_3O_4 NPs is hexagonal when the sample is put on the zone axis of Fe_3O_4 [111]. To further understand how the precursor concentration in the solution affected the shape of the NPs, the reaction time for the precursor concentration of 0.3 M was extended to 3 h. The shape of the Fe_3O_4 NPs was changed from a polyhedron obtained after 2 h of reaction (Figure 4b) to a cube (Figure 4f) with an enlarged size of ∼21 nm.

Adjusting the injection rate of precursor is another way to control the monomer concentration. TEM images of Fe_3O_4 NPs synthesized with the injection rates of 2.5 mL/h and 20 mL/h are shown in Supporting Information Figure S5a,b, respectively. The slower injection rate of 2.5 mL/h, resulting in lower monomer concentration, led to smaller but still cubic Fe_3O_4 NPs. The faster injection rate of 20 mL/h led to polyhedral Fe_3O_4 NPs. The changes in size and shape caused by various injection rates were similar to those caused by adjusting the precursor concentration. The XRD patterns of Fe_3O_4 NPs synthesized with the injection rate of 20 mL/h also revealed the increased intensity of (220) and (440), confirming the change in the preferential crystallographic orientation due to the shape change of Fe_3O_4 NPs, shown in Supporting Information Figure S6. The red line in Figure 3a shows the La Mer model for the formation of Fe_3O_4 polyhedrons. The process in period I is similar to the one with a low injection rate of 10 mL/h (blue line). However, the nucleation occurs earlier due to the high amounts of monomers. For the same reason, the monomer concentration was kept at a high level at the end of period II; therefore, the abundant monomers may simultaneously transfer to various planes and the facet-selective growth would be suppressed to some extent during the early stage of period III. Consequently, the shape of Fe_3O_4 NPs remains polyhedral after 2 h of reaction, as shown in Figure 4b. Both {100} and {110} planes, the two lowest surface energy facets in the spinel structure, become the major terminated planes of the polyhedral Fe_3O_4 NPs, consistent with the observed XRD pattern of the polyhedral NP assembly. On the basis of the surface energy of various planes and the textured XRD pattern, the shape of polyhedral NPs should be similar to the rhombicuboctahedron, an Archimedean solid with 8 triangular and 18 square faces, shown in Supporting Information Figure S7. The similar shape was also found in Cu_2O NPs.[16] Because the faceted planes of {100} and {110} are preferentially parallel to the Si substrate surface, more intense Fe_3O_4 (400) and (220) peaks are observed in the XRD pattern (Figure 4d). The perspective view from the ⟨111⟩ direction of rhombicuboctahedron, shown in Supporting Information Figure S7d, reveals a hexagonal shape which coincides with the 2D projection observed in the HRTEM image along the [111] zone axis, as shown in Figure 4e.

As we show in Figure 3a, the monomer concentration in the reaction solution during period III is important for the final shape in our synthetic system. If the reaction time is extended for the rhombicuboctahedron case so that the monomer concentration in the reaction solution can be continuously decreased to a level at which the differences of the growth rate and dissolution/reconstruction rates between {110} and {100} become substantial, the cubic shape can be obtained, as demonstrated in Figure 4f. On the basis of the shape evolution shown in Figure 3b, the rhombicuboctahedron is an intermediate state, and monomer concentration at the end of period II determines how long the equilibrium shape (cube) can be achieved.

XMCD Analyses of Cation-Site Occupation of Shaped Fe_3O_4 Nanocrystals. Fe_3O_4 has an inverse spinel structure with the formula of $(Fe^{3+})_A(Fe^{2+}Fe^{3+})_BO_4$. Tetrahedral sites (A site, T_d) are occupied by Fe^{3+}, while octahedral sites (B site, O_h) are occupied by equal numbers of Fe^{2+} and Fe^{3+} in bulk Fe_3O_4. The Fe $L_{2,3}$-edge XMCD spectrum of Fe_3O_4 exhibits features of three

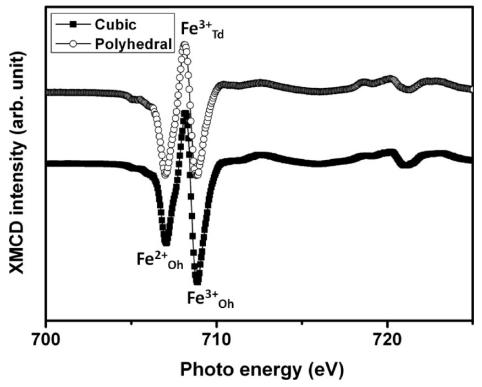

Figure 5. XMCD spectra of cubic and polyhedral Fe_3O_4 NPs.

different chemical environments, namely, $Fe^{3+}_{T_d}$, $Fe^{2+}_{O_h}$, and $Fe^{3+}_{O_h}$. Two major negative peaks, corresponding to $Fe^{2+}_{O_h}$ and $Fe^{3+}_{O_h}$, with a positive peak in between, corresponding to $Fe^{3+}_{T_d}$, were observed;[17] the $Fe^{2+}_{O_h}$ peak at lower photo energy had stronger intensity than the $Fe^{3+}_{O_h}$ one at higher photo energy in the spectrum of bulk Fe_3O_4.[18] The relative peak intensities give the information of cation-site occupancy of Fe_3O_4. Figure 5 shows the normalized XMCD spectra of cubic Fe_3O_4 NPs and polyhedral ones, measured at room temperature. The shape-dependent XMCD spectra of Fe_3O_4 NPs were clearly observed. For the cubic NPs, the maximum peak was contributed by $Fe^{3+}_{O_h}$, while it was reduced in the case of polyhedral NPs. These results indicated that the Fe^{3+} ions were more stable than Fe^{2+} ions at the octahedral sites when the shape of Fe_3O_4 NPs became cubic. Park et al. reported size-dependent XMCD spectra of Fe_3O_4 NPs.[19] They found that the maximum peak of large Fe_3O_4 NPs with a size of 22 nm was contributed by $Fe^{2+}_{O_h}$, similar to bulk Fe_3O_4, whereas the maximum peak of small NPs with a size of 5 nm was contributed by $Fe^{3+}_{O_h}$. Because the sizes of the cubic and polyhedral Fe_3O_4 NPs in our system are similar (~16 nm), the variations of XMCD spectra do not originate from the size effects. Furthermore, the reported XMCD spectra of bulk γ-Fe_2O_3 also show the maximum peak contributed by $Fe^{3+}_{O_h}$. Therefore, it is important to identify whether the observed variations of XMCD spectra in our nanocubes were caused by the shape effect or by the formation of γ-Fe_2O_3. Further characterization to distinguish Fe_3O_4 from γ-Fe_2O_3 was conducted by using X-ray photoelectron spectroscopy (XPS) at room temperature. Supporting Information Figure S8 shows the XPS spectrum of Fe_3O_4 nanocubes. No satellite peak between the peaks of Fe $2p_{3/2}$ and Fe $2p_{1/2}$ was observed, indicating that these nanocubes were composed of Fe_3O_4. Hence, the enhanced intensity of $Fe^{3+}_{O_h}$ in the XMCD spectrum was not attributed to the existence of γ-Fe_2O_3. Both cubic and small Fe_3O_4 NPs have a larger portion of surface atoms (ions) than rhombicuboctahedral and large NPs, respectively. Therefore, the higher surface-to-volume ratio of Fe_3O_4 NPs could presumably be one of the reasons to increase the occupancies of ferric ions, Fe^{3+}, at octahedral sites. In addition, the {001} terminated planes of nanocubes may also lead to the enhanced $Fe^{3+}_{O_h}$ peak. It was reported that the outmost layers composed of B-site layers are relatively more stable than those composed of A-site layers on the Fe_3O_4 (001) surface.[20] The terminated (001) planes are therefore mainly composed of octahedral $Fe_{O_h}{}^{2+}$, $Fe_{O_h}{}^{3+}$, and oxygen irons. The Fe_3O_4 (001) surface was reported to have a higher Fe^{3+}/Fe^{2+} ratio than the bulk.[21] Consequently, the enhanced $Fe^{3+}_{O_h}$ peak in the XMCD spectrum of cubic Fe_3O_4 NPs could be partially attributed to their terminated {100} planes.

CONCLUSION

We have demonstrated that the modified hot-injection method can be successfully used to synthesize the shaped Fe_3O_4 NPs. The cubic Fe_3O_4 NPs with the terminated {100} planes were synthesized when the monomer concentration was low. The shape of the Fe_3O_4 NPs could be changed to rhombicuboctahedral when the monomer concentration was increased by increasing the precursor concentration or by speeding the injection rate. The shape formation mechanism studied by TEM analyses revealed that the nucleation and fast growth occurred in period II in the La Mer model and the final shape of NPs was determined in period III, in which the monomer concentration is a dominant factor. The limited monomers preferentially grew on the planes with high surface energy, leading to the formation of shaped Fe_3O_4 NPs. Furthermore, both cubic and rhombicuboctahedral NPs showed shape-induced in-plane crystallographic orientation-ordered superlattices. Finally, the shape-dependent cation-site occupancies are reported and are ascribed to the terminated plane or the surface-to-volume ratio.

ASSOCIATED CONTENT

Supporting Information. Schematic presentation of the synthetic procedure, size distribution, and XPS spectrum of Fe_3O_4 nanocubes, TEM images for the NPs synthesized with different surfactant concentrations, TEM images and XRD patterns for the NPs synthesized with different injection rate, and pictorial drawing of rhombicuboctahedron. This material is available free of charge via the Internet at http://pubs.acs.org .

AUTHOR INFORMATION

Corresponding Author
*E-mail: chlai@mx.nthu.edu.tw.

ACKNOWLEDGMENT

This research was supported by National Science Council of Republic of China under Grant Nos. NCS 98-2221-E-007-041-MY3 and 99-2923-E-007-003-MY2 and by Ministry of Economic Affairs of Republic of China under Grant No. 98A0177J4.

REFERENCES

(1) (a) Jun, Y. W.; Choi, J. S.; Cheon, J. *Angew. Chem., Int. Ed.* **2006**, *45*, 3414. (b) Lee, S. M.; Cho, S. N.; Cheon, J. *Adv. Mater.* **2003**, *15*, 441. (c) Tao, A. R.; Habas, S.; Yang, P. D. *Small* **2008**, *4*, 310. (d) Xia, Y.; Xiong, Y. J.; Lim, B.; Skrabalak, S. E. *Angew. Chem., Int. Ed.* **2009**, *48*, 60.

(2) (a) Huber, D. L. *Small* **2005**, *1*, 482. (b) Sun, S. H. *Adv. Mater.* **2006**, *18*, 393. (c) Sun, S. H.; Anders, S.; Thomson, T.; Baglin, J. E. E.; Toney, M. F.; Hamann, H. F.; Murray, C. B.; Terris, B. D. *J. Phys. Chem. B* **2003**, *107*, 5419. (d) Sun, S. H.; Fullerton, E. E.; Weller, D.; Murray, C. B. *IEEE Trans. Magn.* **2001**, *37*, 1239. (e) Sun, S. H.; Murray, C. B.; Weller, D.; Folks, L.; Moser, A. *Science* **2000**, *287*, 1989. (f) Sun, S. H.; Zeng, H.; Robinson, D. B.; Raoux, S.; Rice, P. M.; Wang, S. X.; Li, G. X. *J. Am. Chem. Soc.* **2004**, *126*, 273.

(3) (a) Pankhurst, Q. A.; Connolly, J.; Jones, S. K.; Dobson, J. *J. Phys. D: Appl. Phys.* **2003**, *36*, R167. (b) Gupta, A. K.; Gupta, M. *Biomaterials* **2005**, *26*, 3995. (c) Berry, C. C.; Curtis, A. S. G. *J. Phys. D: Appl. Phys.* **2003**, *36*, R198. (d) Berry, C. C. *J. Phys. D: Appl. Phys.* **2009**, *42*, 224003.

(e) Cheon, J. W.; Lee, J. H. *Acc. Chem. Res.* **2009**, *42*, 1907. (f) Cheon, J. W.; Lee, J. H. *Acc. Chem. Res.* **2008**, *41*, 1630.

(4) (a) Zeng, H.; Rice, P. M.; Wang, S. X.; Sun, S. H. *J. Am. Chem. Soc.* **2004**, *126*, 11458. (b) Zheng, R. K.; Gu, H. W.; Xu, B.; Fung, K. K.; Zhang, X. X.; Ringer, S. P. *Adv. Mater.* **2006**, *18*, 2418. (c) Kovalenko, M. V.; Bodnarchuk, M. I.; Lechner, R. T.; Hesser, G.; Schaffler, F.; Heiss, W. *J. Am. Chem. Soc.* **2007**, *129*, 6352. (d) Yang, H.; Hasegawa, D.; Takahashi, M.; Ogawa, T. *IEEE Trans. Magn.* **2008**, *44*, 3895. (e) Yang, H. T.; Ogawa, T.; Hasegawa, D.; Takahashi, M. *J. Appl. Phys.* **2008**, *103*, 07D526. (f) Kim, D.; Lee, N.; Park, M.; Kim, B. H.; An, K.; Hyeon, T. *J. Am. Chem. Soc.* **2009**, *131*, 454. (g) Gao, G.; Liu, X.; Shi, R.; Zhou, K.; Shi, Y.; Ma, R.; Takayama-Muromachi, E.; Qiu, G. *Cryst. Growth Des.* **2010**, *10*, 2888.

(5) Salazar-Alvarez, G.; Qin, J.; Sepelak, V.; Bergmann, I.; Vasilakaki, M.; Trohidou, K. N.; Ardisson, J. D.; Macedo, W. A. A.; Mikhaylova, M.; Muhammed, M.; Baro, M. D.; Nogues, J. *J. Am. Chem. Soc.* **2008**, *130*, 13234.

(6) Mulakaluri, N.; Pentcheva, R.; Wieland, M.; Moritz, W.; Scheffler, M. *Phys. Rev. Lett.* **2009**, *103*, 176102.

(7) Murray, C. B.; Norris, D. J.; Bawendi, M. G. *J. Am. Chem. Soc.* **1993**, *115*, 8706.

(8) Cozzoli, P. D.; Manna, L.; Curri, M. L.; Kudera, S.; Giannini, C.; Striccoli, M.; Agostiano, A. *Chem. Mater.* **2005**, *17*, 1296.

(9) Schladt, T. D.; Graf, T.; Tremel, W. *Chem. Mater.* **2009**, *21*, 3183.

(10) Kendelewicz, T.; Liu, P.; Doyle, C. S.; Brown, G. E.; Nelson, E. J.; Chambers, S. A. *Surf. Sci.* **2000**, *453*, 32.

(11) Song, Q.; Ding, Y.; Wang, Z. L.; Zhang, Z. J. *J. Phys. Chem. B* **2006**, *110*, 25547.

(12) Ostwald, W. *Z. Phys. Chem., Stoechiom. Verwandtschaftsl.* **1900**, *34*, 495.

(13) (a) Peng, X. G. *Adv. Mater.* **2003**, *15*, 459. (b) Manna, L.; Scher, E. C.; Alivisatos, A. P. *J. Am. Chem. Soc.* **2000**, *122*, 12700. (c) Gorshkov, V.; Zavalov, A.; Privman, V. *Langmuir* **2009**, *25*, 7940.

(14) La Mer, V. K.; Dinegar, R. H. *J. Am. Chem. Soc.* **1950**, *72*, 4847.

(15) Song, O.; Zhang, Z. J. *J. Am. Chem. Soc.* **2004**, *126*, 6164.

(16) Zhou, W. W.; Yan, B.; Cheng, C. W.; Cong, C. X.; Hu, H. L.; Fan, H. J.; Yu, T. *CrystEngComm* **2009**, *11*, 2291.

(17) Pearce, C. L.; Henderson, C. M. B.; Pattrick, R. A. D.; van der Laan, G.; Vaughan, D. J. *Am. Mineral.* **2006**, *91*, 880.

(18) Pentcheva, R.; Wendler, F.; Meyerheim, H. L.; Moritz, W.; Jedrecy, N.; Scheffler, M. *Phys. Rev. Lett.* **2005**, *94*, 126101.

(19) Park, J.; An, K. J.; Hwang, Y. S.; Park, J. G.; Noh, H. J.; Kim, J. Y.; Park, J. H.; Hwang, N. M.; Hyeon, T. *Nat. Mater.* **2004**, *3*, 891.

(20) Cheng, C. *Phys. Rev. B* **2005**, *71*, 052401.

(21) Chambers, S. A.; Joyce, S. A. *Surf. Sci.* **1999**, *420*, 111.